HOMO band dispersion of crystalline rubrene: Effects of self-energy corrections within the *GW* approximation

Susumu Yanagisawa,[1,2,*] Yoshitada Morikawa,[2] and Arno Schindlmayr[3]

[1]*Department of Physics and Earth Sciences, Faculty of Science, University of the Ryukyus, 1 Senbaru, Nishihara, Okinawa 903-0213, Japan*
[2]*Department of Precision Science and Technology, Osaka University, 2-1 Yamada-Oka, Suita, Osaka 565-0871, Japan*
[3]*Department Physik, Universität Paderborn, 33095 Paderborn, Germany*

We investigate the band dispersion and relevant electronic properties of rubrene single crystals within the *GW* approximation. Due to the self-energy correction, the dispersion of the highest occupied molecular orbital (HOMO) band increases by 0.10 eV compared to the dispersion of the Kohn-Sham eigenvalues within the generalized gradient approximation, and the effective hole mass consequently decreases. The resulting value of 0.90 times the electron rest mass along the Γ-Y direction in the Brillouin zone is closer to experimental measurements than that obtained from density-functional theory. The enhanced bandwidth is explained in terms of the intermolecular hybridization of the HOMO(Y) wave function along the stacking direction of the molecules. Overall, our results support the bandlike interpretation of charge-carrier transport in rubrene.

I. INTRODUCTION

The electronic properties of organic semiconductors have attracted considerable attention in recent years because of their relevance for light-emitting diodes, photovoltaic cells, field-effect transistors, and other technological applications. They are superior to the prevailing inorganic devices due to their low power consumption, low-cost and large-area fabrication, and flexibility.[1]

A detailed understanding of the charge-carrier transport in organic semiconductors is of crucial importance for the optimization of device performances. In contrast to the band transport typically encountered in inorganic crystals, transport in organic materials is often explained in the hopping or polaronic picture, where the charge carriers are strongly coupled to local lattice deformations. Experiments can, in principle, distinguish between the two mechanisms, but to clarify the intrinsic electronic properties without impurities or lattice defects, single crystals of organic semiconductors must be studied.

Charge-carrier transport in single crystals of rubrene (5,6,11,12-tetraphenyltetracene) has been the focus of such studies, which found a hole mobility of 40 cm^2/V s, the highest reported value among all organic semiconductors,[2] and also noted the strong anisotropy of the conductivity, which reflects the underlying crystal structure.[3–5] The experiments furthermore pointed toward a bandlike transport, based on the temperature dependence of the hole mobility and the Hall effect.[6–8]

Recently, the dispersion of the highest occupied molecular orbital (HOMO) band of rubrene was measured using angle-resolved ultraviolet photoelectron spectroscopy (ARUPS).[9] A significant dispersion with a bandwidth of 0.4 eV along the Γ-Y direction in the Brillouin zone, which corresponds to the orientation of the molecular stacking, and almost no dispersion along Γ-X were observed. These results are in agreement with other photoemission studies[10,11] as well as band-structure calculations within density-functional theory (DFT).[12–14] In addition, the noticeably light effective mass deduced from the

ARUPS data, which was estimated to be 0.65 ± 0.1 of the electron rest mass,[9] provides further strong evidence in favor of the band transport of the holes.

While the bandlike picture thus seems well-supported, many theoretical investigations of transport in rubrene still adhere to the polaron picture in order to explain the high mobility and anisotropy of the hole transport, using semiclassical dynamics and parameters obtained from first-principles simulations of single molecules or dimers.[15–17] If the electron-phonon coupling indeed plays a significant role, as claimed in these studies, then it should not only have a detectable effect on the temperature dependence of the carrier mobility and transport properties, but also modify the electronic band structure. For example, in pentacene single crystals, where the bandwidths obtained from DFT or from the *GW* approximation for the electronic self-energy[18] turn out to be significantly smaller than experimentally observed,[19–21] the inclusion of the electron-phonon coupling and energy fluctuations by disorder are indispensable to reach quantitative agreement with photoemission measurements.[22]

Although the reported DFT band structures[12–14] appear to reproduce the ARUPS data well without any electron-phonon coupling in the case of rubrene, the Kohn-Sham eigenvalues of DFT are known to differ systematically from the actual quasiparticle energies, so that the good agreement could be fortuitous. For a better understanding of the still controversial mechanism of the carrier transport in rubrene, more insight from higher-level first-principles electronic-structure methods is hence necessary. Although there are already calculations of the quasiparticle energy gap within the *GW* approximation,[23,24] no theoretical studies of the band dispersion beyond DFT have been reported until now.

Here we investigate the band structure of rubrene single crystals within the *GW* approximation. We find that the HOMO band dispersion is enhanced due to the self-energy correction, leading to a lighter effective hole mass compared to the DFT value in good agreement with photoemission data. From our results we conclude that the hole carrier transport
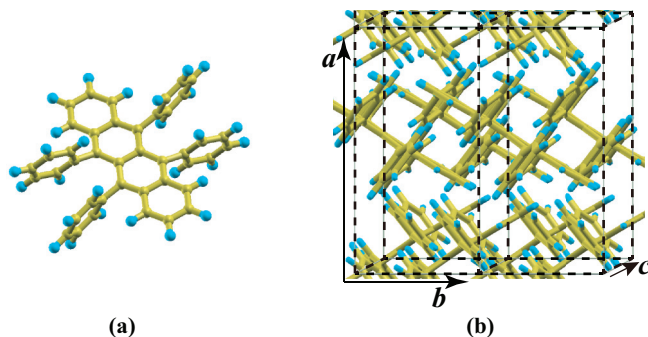
FIG. 1. (Color online) Atomic structure of (a) isolated rubrene molecules and (b) rubrene single crystals. The C and H atoms are indicated by yellow and light blue spheres, respectively. In the single crystal, the tilted long axes of the molecules are stacked along the b direction.

along the Γ-Y direction is indeed bandlike, as experimentally suggested.

II. COMPUTATIONAL METHOD

The atomic structure of rubrene is illustrated in Fig. 1. The orthorhombic unit cell of the single crystal contains four rubrene molecules, thereby comprising a total of 280 atoms, in a herringbone-like stacked arrangement with the space-group symmetry $Cmca$. We use the experimental lattice constants[25] $a = 14.1289$ Å, $b = 7.145\,50$ Å, and $c = 26.7450$ Å. This choice deviates from the standard $Cmca$ setting, where the largest lattice parameter corresponds to a, in order to facilitate a comparison with Ref. 9. The DFT calculations are performed with the STATE code.[26] We use norm-conserving pseudopotentials,[27] a plane-wave basis set with a cutoff energy of 72 Ry, and the Perdew-Burke-Ernzerhof (PBE) exchange-correlation functional.[28] The Brillouin zone is sampled with $1 \times 2 \times 1$ Γ-centered **k** points. The atomic positions inside the unit cell are relaxed until the maximum force drops below a threshold value of 0.08 nN. For this geometry optimization, we additionally include a semiempirical treatment of the van der Waals contribution to the total energy.[29]

We calculate the band structure along the path Z-Γ-Y-X-Γ, where Γ-X corresponds to the a crystal axis and Γ-Y to the b axis in real space. The effective masses are then obtained by fitting the top of the HOMO band with parabolic functions. For this purpose, we evaluate the band energies on a dense mesh around Γ with a spacing of 0.027 and 0.028 Å^{-1} along the Γ-Y and Γ-X directions, respectively.

Besides the DFT-PBE treatment, we also calculate more accurate quasiparticle energies including self-energy corrections within the non-self-consistent GW (G_0W_0) approximation, using the GW space-time code.[30–32] Unlike traditional reciprocal-space implementations, which typically restrict the calculation of quasiparticle energies to the preselected global **k**-point set, this real-space algorithm allows an easy evaluation of self-energy corrections at arbitrary wave vectors, as is required here to sample the band curvature. The same approach was successfully used to determine the effective electron mass in strained silicon, in good agreement with experiments.[33,34]

As in other G_0W_0 calculations for similar systems,[23,24] the noninteracting Green function G_0 is constructed here with the PBE wave functions and eigenvalues. We apply cutoff energies of 60 and 24 Ry for the static exchange and the dynamical correlation self-energy, respectively. Instead of plasmon-pole models, which are still widely used in practical G_0W_0 calculations, especially for large systems,[36] we evaluate the full frequency dependence of the dielectric screening function numerically within the random-phase approximation. In the sum over states, we include 11 200 bands, which includes all unoccupied bands up to about 145 eV above the Fermi level. With these parameters, the HOMO bandwidth is converged to within 0.02 eV.[35] The lowest unoccupied molecular orbital (LUMO) band converges more slowly, however: Its width is converged only to within 0.1 eV with the same set of parameters, which does not allow us to reliably estimate the effective electron mass. Based on our convergence tests, we further estimate that the band gap increases by about 0.1 eV if the number of **k** points is doubled to $2 \times 4 \times 2$.

III. RESULTS AND DISCUSSION

Figure 2 shows the band dispersions calculated within both PBE and G_0W_0. In addition, Table I contains the numerical values of the bandwidths, the energy gap, and the valence-band splitting. The strong anisotropy of the dispersion along the different principal axes in reciprocal space, which is linked to the anisotropic mobility of the charge carriers observed in experiments,[3–5] is clearly visible. Quantitatively, the direct band gap of 1.13 eV at Γ obtained within PBE agrees with other calculations at the same level of theory.[23,24] Likewise,
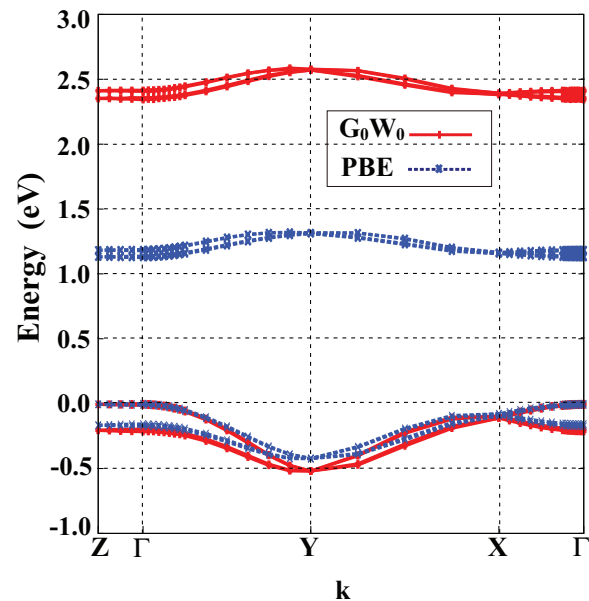
FIG. 2. (Color online) PBE and G_0W_0 band structure of the eight bands (HOMO-3 to LUMO$+3$) along Z-Γ-Y-X-Γ in the Brillouin zone. The HOMO energy at Γ is set to zero. There are four pairs of degenerate bands that originate from the two inequivalent molecule pairs in adjacent ab planes separated by a distance $c/2$. The calculated data points, indicated by symbols, are connected by lines to guide the eye.

TABLE I. HOMO and LUMO bandwidths W_{HOMO} and W_{LUMO} along Γ-Y and Γ-X, direct band gap $E_{\text{g}}(\Gamma)$, and valence-band splitting $\Delta(\Gamma)$ in rubrene single crystals in eV.

	PBE	G_0W_0	References
$W_{\text{HOMO}}(\Gamma\text{-Y})$	0.42	0.52	0.4[a]
$W_{\text{HOMO}}(\Gamma\text{-X})$	0.08	0.10	<0.05[a]
$W_{\text{LUMO}}(\Gamma\text{-Y})$	0.18	0.23	
$W_{\text{LUMO}}(\Gamma\text{-X})$	0.03	0.04	
$E_{\text{g}}(\Gamma)$	1.13	2.34	2.5[b]
$\Delta(\Gamma)$	0.16	0.20	

[a]Reference 9; ARUPS measurement.
[b]Reference 24; G_0W_0.

the HOMO bandwidth of 0.42 eV along Γ-Y is in accordance with previous density-functional results,[12–14] as is the small but finite bandwidth of 0.08 eV along Γ-X. Minor discrepancies arise from differences in the computational procedures and setups, such as the choice of exchange-correlation functional or variations in the structural configuration. For example, unlike in previous studies, we include here the van der Waals interaction between the molecules when relaxing the atomic positions inside the unit cell.

To obtain a more accurate band structure, we apply the G_0W_0 approximation. The results are included in Fig. 2 and Table I. The quasiparticle band gap of 2.34 eV is larger than the PBE eigenvalue gap by 1.21 eV and in good agreement with a recently reported value[24] of 2.5 eV. On the other hand, as already pointed out in Ref. 24, this is appreciably smaller than the G_0W_0 band gap of 2.8 eV obtained for a model unit cell with higher symmetry and reduced volume that contains only two instead of four rubrene molecules.[23] No direct measurement of the fundamental band gap is available, but our result is close to the optical gap of 2.2 eV deduced from infrared transmission spectra,[13] a related but slightly smaller quantity that differs from the quasiparticle band gap only by the exciton binding energy. Based on this optical gap and our own calculated band gap of 2.34 eV, along with another reported G_0W_0 result[24] of 2.5 eV, the exciton binding energy in rubrene can be estimated as 0.1–0.3 eV, slightly smaller than the theoretical binding energy of 0.5 eV obtained from a solution of the Bethe-Salpeter equation.[23] Although the latter result may be influenced by the different unit cell used in Ref. 23, we note that a very similar value of about 0.5 eV was also predicted for pentacene within the same framework.[36]

As a consequence, it may appear as if the band gap of rubrene obtained in this work or in Ref. 24 was slightly underestimated. The deviations are within the expected error bar of a G_0W_0 calculation, however, which may amount to a few tenths of an eV for a highly complex system such as rubrene, as illustrated by our own convergence tests described above. Small variations in the calculated band gaps may arise from technical details, such as the use of pseudopotentials, the treatment of the frequency dependence of the dielectric function in the self-energy, or from the convergence with respect to the plane-wave cutoff, the **k**-point sampling, and, in particular, the number of unoccupied bands in the spectral sum. Larger band gaps can also be obtained by using single-particle wave functions and eigenvalues from hybrid functionals, or

by a partially self-consistent construction of the self-energy.[36] However, it is not easy to apply such modifications in the case of rubrene because of the large system size and the associated high computational cost.

Although the important role of self-energy corrections for an accurate quantitative description of the band structure is beyond doubt, there are some other aspects of band-gap calculations within the G_0W_0 approximation that should be borne in mind. As discussed in a recent study of bulk pentacene,[36] for a proper comparison of the G_0W_0 bulk band gap of organic solids with photoemission data, it may be necessary to take physical effects such as the incomplete charge screening at the surface, static and dynamical structural disorder, or the finite experimental resolution, which influence all measurements but are not reflected in the theoretical calculations, into account. Furthermore, the electron-phonon coupling, which tends to decrease the band gaps of semiconductors,[37] may also be significant. For the moment, we do not consider these issues further. Instead, having confirmed that self-energy corrections lead to a vastly improved band gap, we now proceed to investigate the bandwidths.

The basic character of the dispersion is retained after self-energy corrections within the G_0W_0 approximation are included: The HOMO band exhibits a large dispersion along Γ-Y and is almost flat along Γ-X. However, the calculated bandwidth of 0.52 eV along Γ-Y is 0.10 eV larger than the PBE value, while the dispersion along Γ-X also increases slightly. This increase in the bandwidth due to the self-energy correction is consistent with the results for pentacene single crystals.[19] The same systematic behavior was also reported for solid C_{60} and a variety of inorganic insulators.[38]

Table II shows the relevant matrix elements of the PBE exchange-correlation potential V_{xc}, the static exchange (Σ_{x}), and the dynamical correlation (Σ_{c}) part of the self-energy as well as the sum $\Sigma = \Sigma_{\text{x}} + \Sigma_{\text{c}}$ for the HOMO and the LUMO band energies at Γ, Y, and X. The difference $\Sigma - V_{\text{xc}}$ amounts to about 1.1 eV for all states in the LUMO band but is much smaller for states in the HOMO band, so that the widening of the band gap due to the G_0W_0 self-energy correction stems almost entirely from an upward shift of the former. Upon closer inspection, one finds that $\Sigma - V_{\text{xc}}$ varies within the HOMO band as a function of **k** between -0.13 eV at Γ, the top of the band, and -0.23 eV at Y, the bottom of the band. Thus the separation between the band edges grows, which leads to an overall increase in the bandwidth. The magnitude of the

TABLE II. Contribution of the PBE exchange-correlation potential V_{xc}, static exchange Σ_{x}, dynamical correlation Σ_{c}, and the total G_0W_0 self-energy $\Sigma = \Sigma_{\text{x}} + \Sigma_{\text{c}}$ to the HOMO and LUMO band energies at Γ, Y, and X in eV.

	V_{xc}	Σ_{x}	Σ_{c}	Σ
HOMO(Γ)	-14.50	-15.10	0.47	-14.64
HOMO(Y)	-13.91	-14.84	0.70	-14.14
HOMO(X)	-14.37	-15.02	0.50	-14.52
LUMO(Γ)	-13.67	-9.44	-3.14	-12.58
LUMO(Y)	-13.81	-9.44	-3.24	-12.69
LUMO(X)	-13.70	-9.46	-3.14	-12.60

matrix elements at Y is also noticeably smaller than at the other points.

The underlying reason for the observed behavior is the different spatial nature of the orbitals for wave vectors across the Brillouin zone. As a general rule, wave functions that are more concentrated at the atomic positions, where the electron density is highest, correspond to larger negative matrix elements of local or semilocal exchange-correlation potentials. As states at the bottom of a fully occupied valence

band are bonding linear combinations of atomic or molecular orbitals with a large amplitude in the interjacent space, whereas the states at the top of the band are antibonding linear combinations with a node between the sites, exchange and correlation strongly compress the band in DFT. Within the G_0W_0 approximation, this effect is less pronounced due to the nonlocal nature of the self-energy. Therefore, the quasiparticle correction removes part of the excessive compression, thus yielding increased bandwidths that are typically in better
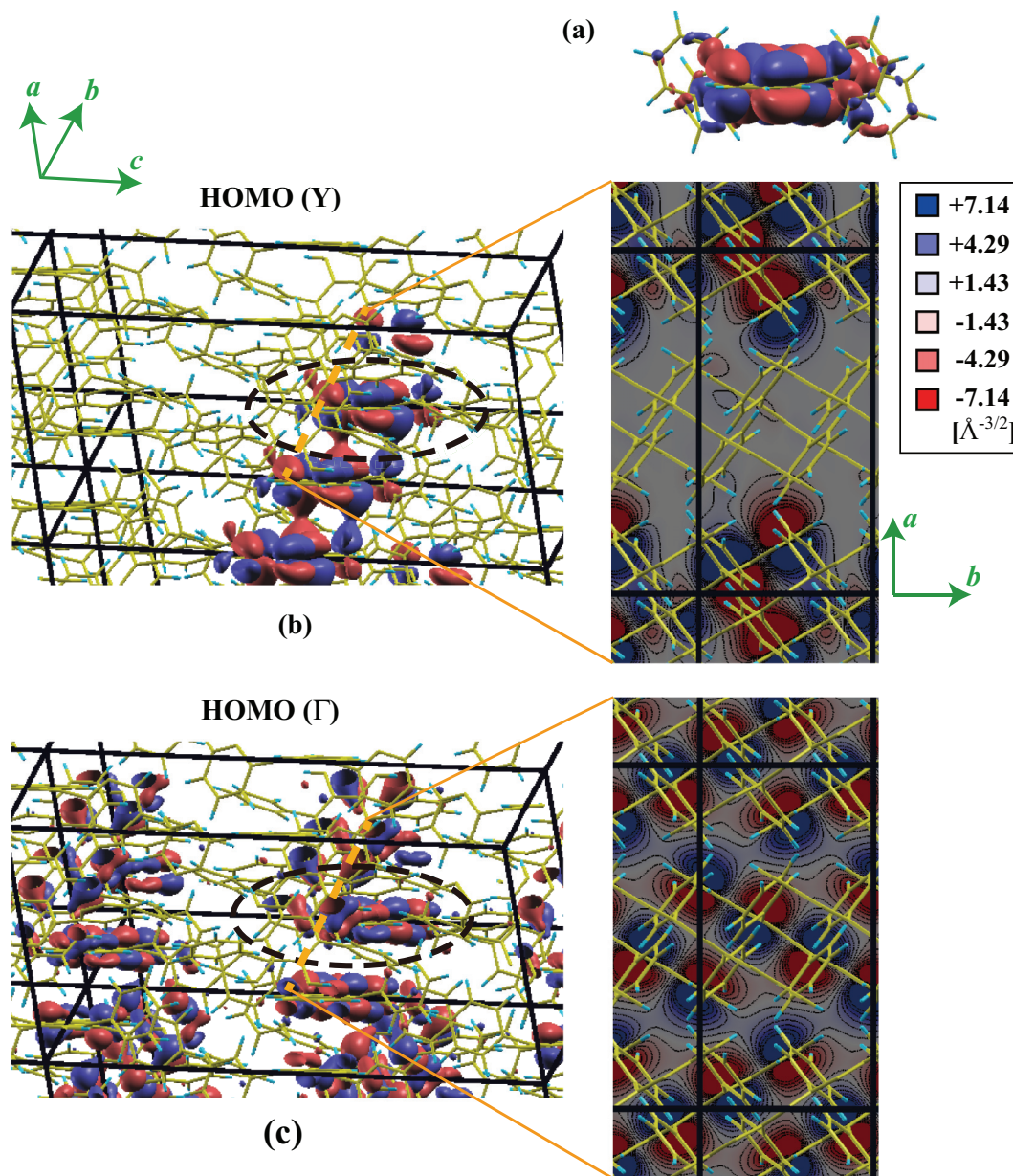
FIG. 3. (Color online) Isosurfaces of the HOMO wave function (real part) of (a) an isolated rubrene molecule as well as (b) HOMO(Y) and (c) HOMO(Γ) in a single crystal. The atomic configuration and orientation in (a) are identical to the molecular units in the single crystal, indicated by the black dashed circle in (b) and (c). The amplitude of the isosurfaces is ± 7.14 Å$^{-3/2}$, and different colors indicate the sign. In addition, contour plots in the ab plane cutting through the orange dashed lines in (b) and (c), along which the largest concentration of the isosurfaces is located, are displayed. The black solid lines mark the unit cell. Note that HOMO(Y), which is centered on one of the four molecules in the unit cell, is degenerate with each of the HOMO−3(Y) to HOMO−1(Y) states, which are centered on the other three molecules and exhibit a similar spatial distribution. Some of the isosurfaces in the left panels of (b) and (c) are truncated in order to avoid excessive overlap and improve the visual clarity of the plots.

(a)

(b) **HOMO−1(Y)**

+7.14
+4.29
+1.43
−1.43
−4.29
−7.14
[Å$^{-3/2}$]
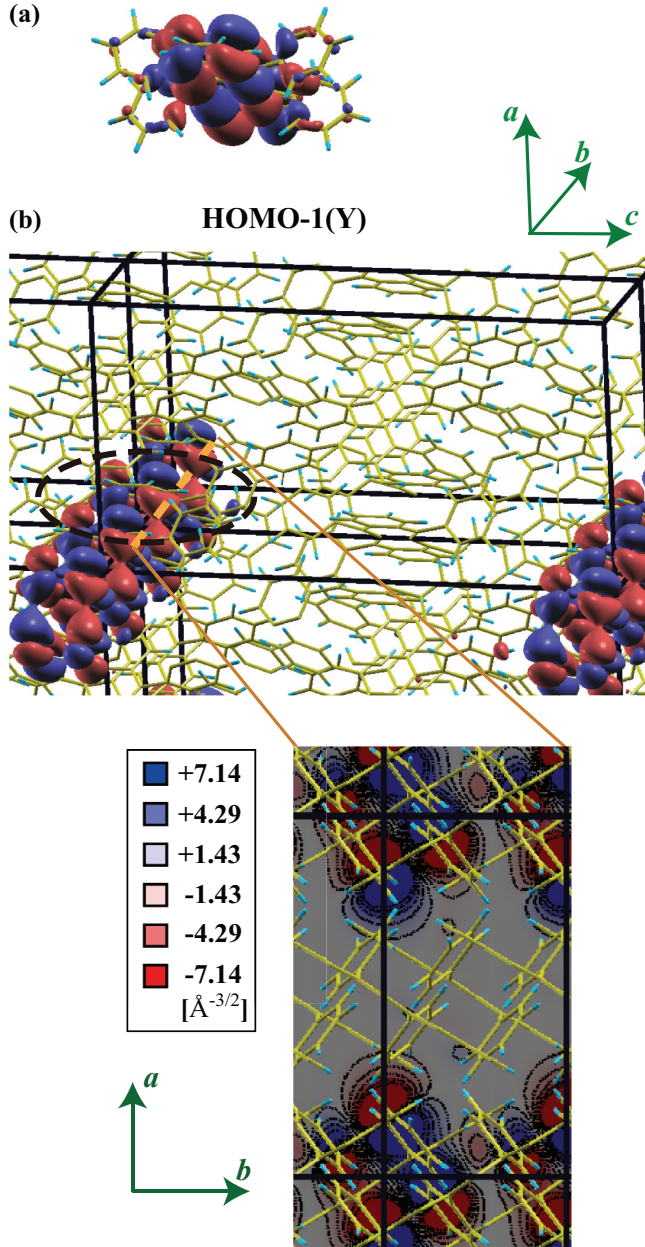
FIG. 4. (Color online) Isosurfaces of the HOMO−1 wave function (real part) of (a) an isolated rubrene molecule as well as (b) HOMO−1(Y) in a single crystal. See the explanation of Fig. 3 for details.

agreement with experiments.[38] In our case, both the PBE and the G_0W_0 results are close to the measured value[9–11] of 0.4 eV for rubrene, however.

Figure 3 shows the isosurfaces of the HOMO band wave functions at Γ and Y together with the HOMO of the isolated rubrene molecule for comparison. As expected, the wave function at Γ, illustrated in Fig. 3(c), features no significant hybridization between the molecules because of the antibonding out-of-phase superposition of the orbitals, confirming that the wave function is concentrated at the molecular sites. In contrast, the HOMO state at Y, displayed in Fig. 3(b), exhibits strong hybridization as a result of the

TABLE III. Effective hole mass in rubrene single crystals obtained from the HOMO band dispersion along Γ-Y and Γ-X relative to the electron rest mass.

	PBE	G_0W_0	References
m_h^*/m_e (Γ-Y)	1.00	0.90	0.8 ± 0.1,[a] 0.65 ± 0.1[b]
m_h^*/m_e (Γ-X)	2.15	1.65	1.9 ± 0.3[a]

[a]Reference 13; optical conductivity measurement.
[b]Reference 9; ARUPS measurement.

bonding in-phase superposition, which leads to a lower concentration at individual molecules. The fact that the HOMO(Γ) wave function is more concentrated at the molecular sites is consistent both with the larger matrix elements of V_{xc} listed in Table II and with the upward shift of 0.10 eV relative to the HOMO(Y) state due to the self-energy correction. It is then natural to assume that the hybridization of the HOMO(Y) wave function over molecules stacked along the b axis also underlies the observed conduction channel along this direction. An equivalent spatial distribution is found for the HOMO−1(Y) to HOMO−3(Y) states, which are degenerate with HOMO(Y) but whose wave functions are each centered on another of the four molecules in the unit cell; see Fig. 4 for HOMO−1(Y) as an example.

Along Γ-X, the HOMO bandwidth calculated within G_0W_0 is 0.10 eV, marginally larger than the PBE value of 0.08 eV, while experiments observed an essentially flat band with a dispersion smaller than 0.05 eV.[9] As the energy resolution of the ARUPS measurement exceeds 0.1 eV, the predicted finite bandwidth may suggest that factors absent in the present calculation, such as thermal or polaron effects, could still play a role, albeit on a small absolute scale. The splitting of the valence bands at Γ, which results from the coupling between the inequivalent molecules, is 0.16 eV at the PBE level, in agreement with previous calculations[12–14] and slightly enhanced by 0.04 eV as a result of the self-energy correction. No such splitting was observed in photoemission experiments.[9–11] In addition to thermal effects at room temperature, which weaken the coupling, final-state effects may be relevant for this behavior, because the interaction of a localized molecular state with the hole generated upon the emission of an electron could affect the photoemission results, an aspect not explicitly incorporated into the many-body treatment of the crystalline states in this work.

We find that the G_0W_0 self-energy correction may be approximated by a so-called "scissors" operator as previously discussed in a similar study of pentacene.[19,36] If the HOMO(Γ) energy is set to zero as in Fig. 2, then our calculated HOMO and LUMO band dispersions for rubrene are reproduced within 0.02 eV by $\epsilon_{nk}^{GW} = \epsilon_{nk}^{PBE} \times 1.21$ for the HOMO, and by $\epsilon_{nk}^{GW} = \epsilon_{nk}^{PBE} \times 1.17 + 1.02$ eV for the LUMO band. While the stretch factors are very similar to those for pentacene in Ref. 19, our LUMO band shift is somewhat smaller.

Finally, Table III displays the effective hole masses relative to the electron rest mass. The effective masses along Γ-X and Γ-Y differ almost by a factor of 2, reflecting the highly anisotropic carrier mobility. Our PBE results are similar to the values given in another recent theoretical study[14] of the rubrene band structure that employed the B3LYP/6-31G

exchange-correlation functional. As a consequence of the enhanced dispersion and HOMO band curvature, the inclusion of self-energy corrections in the G_0W_0 approximation leads to smaller effective masses. The reduction amounts to more than 10% and brings the results closer to the measured values from the optical conductivity[13] and ARUPS[9] measurements.

As explained above, the results presented in this work are obtained using the experimental lattice constants[25] rather than optimized theoretical lattice parameters determined by a total-energy minimization. Another theoretical work indicated that the lattice constants optimized by using a first-principles nonlocal van der Waals density functional[39–41] are in agreement with experiments with the deviations being within 1%, and the resulting band structure is similar to that at the experimental lattice constants.[42] This result supports the validity of employing the experimental lattice constants. In this context, we note that Ref. 14 found modest changes in the effective masses when the lattice parameters were varied in order to simulate thermal expansion. We would like to leave it to future work to examine the effects of temperature at this level of theory.

IV. CONCLUSIONS

In summary, we have calculated the quasiparticle band structure of rubrene single crystals across the entire Brillouin zone. Unlike in previous studies, self-energy corrections within the G_0W_0 approximation were fully taken into account. While the qualitative features of the band structure, such as the large dispersion along Γ-Y and the almost nondispersive behavior along Γ-X, are preserved, this yields a larger,

improved band gap and also enhances the dispersion of the HOMO band by 0.10 eV relative to the DFT-PBE eigenvalues. These findings were elucidated in terms of the different spatial distribution of the HOMO wave functions at Y and Γ on the molecular sites and the size of the corresponding matrix elements of the self-energy correction. The enhanced HOMO bandwidth obtained within G_0W_0 furthermore leads to a reduced effective hole mass that improves the agreement with the experimental data. Our results support the bandlike picture of transport in rubrene, where the central features of the electronic structure and carrier mobility are explained in terms of purely electronic processes, and the coupling to lattice deformations plays a minor role.

*shou@sci.u-ryukyu.ac.jp

[1] S. R. Forrest, Nature (London) **428**, 911 (2004).

[2] J. Takeya, M. Yamagishi, Y. Tominari, R. Hirahara, Y. Nakazawa, T. Nishikawa, T. Kawase, T. Shimoda, and S. Ogawa, Appl. Phys. Lett. **90**, 102120 (2007).

[3] V. C. Sundar, J. Zaumseil, V. Podzorov, E. Menard, R. L. Willett, T. Someya, M. E. Gershenson, and J. A. Rogers, Science **303**, 1644 (2004).

[4] M.-M. Ling, C. Reese, A. L. Briseno, and Z. Bao, Synth. Met. **157**, 257 (2007).

[5] A. Saeki, S. Seki, T. Takenobu, Y. Iwasa, and S. Tagawa, Adv. Mater. **20**, 920 (2008).

[6] V. Podzorov, E. Menard, A. Borissov, V. Kiryukhin, J. A. Rogers, and M. E. Gershenson, Phys. Rev. Lett. **93**, 086602 (2004).

[7] V. Podzorov, E. Menard, J. A. Rogers, and M. E. Gershenson, Phys. Rev. Lett. **95**, 226601 (2005).

[8] J. Takeya, K. Tsukagoshi, Y. Aoyagi, T. Takenobu, and Y. Iwasa, Jpn. J. Appl. Phys. **44**, L1393 (2005).

[9] S.-I. Machida, Y. Nakayama, S. Duhm, Q. Xin, A. Funakoshi, N. Ogawa, S. Kera, N. Ueno, and H. Ishii, Phys. Rev. Lett. **104**, 156401 (2010).

[10] A. Vollmer, R. Ovsyannikov, M. Gorgoi, S. Krause, M. Oehzelt, A. Lindblad, N. Mårtensson, S. Svensson, P. Karlsson,

M. Lundvuist, T. Schmeiler, J. Pflaum, and N. Koch, J. Electron Spectrosc. Relat. Phenom. **185**, 55 (2012).

[11] Y. Nakayama, Y. Uragami, S. Machida, K. R. Koswattage, D. Yoshimura, H. Setoyama, T. Okajima, K. Mase, and H. Ishii, Appl. Phys. Express **5**, 111601 (2012).

[12] D. A. da Silva Filho, E.-G. Kim, and J.-L. Brédas, Adv. Mater. **17**, 1072 (2005).

[13] Z. Q. Li, V. Podzorov, N. Sai, M. C. Martin, M. E. Gershenson, M. Di Ventra, and D. N. Basov, Phys. Rev. Lett. **99**, 016403 (2007).

[14] Y. Li, V. Coropceanu, and J.-L. Brédas, J. Phys. Chem. Lett. **3**, 3325 (2012).

[15] G. Nan, X. Yang, L. Wang, Z. Shuai, and Y. Zhao, Phys. Rev. B **79**, 115203 (2009).

[16] S.-H. Wen, A. Li, J. Song, W.-Q. Deng, K.-L. Han, and W. A. Goddard, III, J. Phys. Chem. B **113**, 8813 (2009).

[17] H. Tamura, M. Tsukada, H. Ishii, N. Kobayashi, and K. Hirose, Phys. Rev. B **86**, 035208 (2012).

[18] L. Hedin, Phys. Rev. **139**, A796 (1965).

[19] M. L. Tiago, J. E. Northrup, and S. G. Louie, Phys. Rev. B **67**, 115212 (2003).

[20] K. Hummer and C. Ambrosch-Draxl, Phys. Rev. B **72**, 205205 (2005).

[21]H. Kakuta, T. Hirahara, I. Matsuda, T. Nagao, S. Hasegawa, N. Ueno, and K. Sakamoto, Phys. Rev. Lett. **98**, 247601 (2007).

[22]S. Ciuchi, R. C. Hatch, H. Höchst, C. Faber, X. Blase, and S. Fratini, Phys. Rev. Lett. **108**, 256401 (2012).

[23]N. Sai, M. L. Tiago, J. R. Chelikowsky, and F. A. Reboredo, Phys. Rev. B **77**, 161306(R) (2008).

[24]J. A. Berger, L. Reining, and F. Sottile, Phys. Rev. B **85**, 085126 (2012).

[25]J. Takeya (unpublished).

[26]Y. Morikawa, H. Ishii, and K. Seki, Phys. Rev. B **69**, 041403 (2004).

[27]N. Troullier and J. L. Martins, Phys. Rev. B **43**, 1993 (1991).

[28]J. P. Perdew, K. Burke, and M. Ernzerhof, Phys. Rev. Lett. **77**, 3865 (1996).

[29]S. Grimme, J. Comput. Chem. **27**, 1787 (2006).

[30]M. M. Rieger, L. Steinbeck, I. D. White, H. N. Rojas, and R. W. Godby, Comput. Phys. Commun. **117**, 211 (1999).

[31]L. Steinbeck, A. Rubio, L. Reining, M. Torrent, I. D. White, and R. W. Godby, Comput. Phys. Commun. **125**, 105 (2000).

[32]C. Freysoldt, P. Eggert, P. Rinke, A. Schindlmayr, R. W. Godby, and M. Scheffler, Comput. Phys. Commun. **176**, 1 (2007).

[33]S. F. Feste, T. Schäpers, D. Buca, Q. T. Zhao, J. Knoch, M. Bouhassoune, A. Schindlmayr, and S. Mantl, Appl. Phys. Lett. **95**, 182101 (2009).

[34]M. Bouhassoune and A. Schindlmayr, Phys. Status Solidi C **7**, 460 (2010).

[35]We checked the convergence of the calculated band gap and bandwidths with respect to the plane-wave cutoff, the **k**-point sampling, and the sum over bands by varying one of these parameters at a time while keeping all others fixed. The static exchange and the dynamical correlation part are examined separately. We increase the parameters up to $4 \times 8 \times 2$**k** points and a plane-wave cutoff $E_{\text{cut}}^{\text{x}}$ of 72 Ry for the static exchange, and up to $2 \times 4 \times 2$**k** points, a plane-wave cutoff $E_{\text{cut}}^{\text{c}}$ of 32 Ry, and 11 200 bands for the dynamical correlation part. For the convergence with respect to the number of unoccupied bands N_{b}, we fit the computed bandwidths to a linear or quadratic polynomial of $1/N_{\text{b}}$. Such polynomials conform to a recent analytical study[43] and describe well the convergence behavior of the valence bandwidths of Si and zinc-blende GaN calculated with the same code.[31] Indeed, the behavior of the rubrene HOMO bandwidth here is similar to that of Si and GaN in Ref. 31. We estimate that the HOMO bandwidth calculated with $N_{\text{b}} = 11\,200$ is larger by 0.02 eV (Γ-Y) and 0.01 eV (Γ-X) than for $N_{\text{b}} \rightarrow \infty$. For the other parameters besides N_{b}, numerical convergence is achieved within the tested parameter ranges, and their effects on the HOMO bandwidth tend to cancel. Overall, we conclude that the HOMO bandwidth is converged to within 0.02 eV for the parameter set of $1 \times 2 \times 1$**k** points, $E_{\text{cut}}^{\text{x}}$ of 60 Ry and $E_{\text{cut}}^{\text{c}}$ of 24 Ry, and $N_{\text{b}} = 11\,200$ used in this work.

[36]S. Sharifzadeh, A. Biller, L. Kronik, and J. B. Neaton, Phys. Rev. B **85**, 125307 (2012).

[37]M. Cardona and M. L. W. Thewalt, Rev. Mod. Phys. **77**, 1173 (2005).

[38]E. L. Shirley, Phys. Rev. B **58**, 9579 (1998).

[39]K. Lee, É. D. Murray, L. Kong, B. I. Lundqvist, and D. C. Langreth, Phys. Rev. B **82**, 081101(R) (2010).

[40]V. R. Cooper, Phys. Rev. B **81**, 161104(R) (2010).

[41]I. Hamada and M. Otani, Phys. Rev. B **82**, 153412 (2010).

[42]I. Hamada (unpublished).

[43]A. Schindlmayr, Phys. Rev. B **87**, 075104 (2013).